Nuclear Science and Techniques (2025) 36:80
https://doi.org/10.1007/s41365-025-01645-z

Beam flux measurement using a photon activation analysis method at the SLEGS

Yu-Xuan Yang[1,2] · Yue Zhang[3] · Zhi-Cai Li[3,4] · Zi-Rui Hao[3] · Sheng Jin[2,5] · Kai-Jie Chen[2,6] · Zhen-Wei Wang[2,5] · Qian-Kun Sun[2,5] · Gong-Tao Fan[2,3,5] · Hang-Hua Xu[3] · Long-Xiang Liu[3] · Wei-Juan Zhao[1] · Hong-Wei Wang[2,3,5]

Received: 5 February 2024 / Revised: 13 June 2024 / Accepted: 5 July 2024 / Published online: 20 March 2025

Abstract

The Shanghai Laser Electron Gamma Source (SLEGS) delivers quasi-monochromatic, continuously energy-tunable γ-ray beams. Based on a Photon Activation Analysis (PAA) method, SLEGS built and developed a photon activation analysis platform, including online activation and offline low background High-Purity Germanium (HPGe) detector measurement systems, as an alternative to direct measurement methods and low-throughput cross-tests. Owing to short half-lives spanning from minutes to days and characteristics such as ease of fabrication, cost-effectiveness, and stability, gold (^{197}Au) and zinc (^{64}Zn) emerge as favorable activation targets for the γ-ray beam flux monitor. Notably, they exhibit a multitude of advantages in monitoring the γ-ray beam flux, typically 10^5 photons/s, with energies of 13.16 MeV to 19.08 MeV using a 3 mm coarse collimator. In particular, high-flux γ-ray beam experiments can be conducted effectively.

Keywords SLEGS · Laser Compton scattering · Beam flux · Photon activation analysis

1 Introduction

The Shanghai Laser Electron Gamma Source (SLEGS) is a beamline station constructed in the Shanghai Synchrotron Radiation Facility (SSRF) project II. The SLEGS is the first pioneering Laser Compton Slanting Scattering (LCSS) gamma source, and it is characterized by its innovative approach of employing a continuously changing collision angle of 20 degrees to 160 degrees, which can produce an adjustable γ-ray energy within the range of 660 keV to 21.7 MeV [1–3]. The SLEGS is an important platform for basic and applied scientific research in photonuclear physics [4–8]. The γ-ray beam flux is a crucial parameter for the SLEGS, and its measurement can be accomplished through direct or indirect measurements via a photonuclear reaction. Large-volume scintillator detectors such as $LaBr_3$(Ce), BGO, and NaI(Tl) detector offer direct measurements by attenuating the γ-ray beam intensity. However, limitations arise at high count rates (less than 10^6 cps) because of the long decay time of scintillators and limited readout rate of PMTs. The plastic scintillator paddle detectors employed at the High Intensity Gamma-ray Source (HIγS) allow beam flux measurements of up to 3×10^7 photons/s, with an accuracy of at least 2% [9].

This work was supported by National Key Research and Development Program of China (Nos. 2022YFA1602404 and 2023YFA1606901), the National Natural Science Foundation of China (Nos. 12275338, 12388102, and U2441221), and the Key Laboratory of Nuclear Data Foundation (JCKY2022201C152).

✉ Wei-Juan Zhao
zwj@zzu.edu.cn

✉ Hong-Wei Wang
wanghw@sari.ac.cn

1 School of Physics, Zhengzhou University, Zhengzhou 450001, China

2 Shanghai Institute of Applied Physics, Chinese Academy of Sciences, Shanghai 201800, China

3 Shanghai Advanced Research Institute, Chinese Academy of Sciences, Shanghai 201210, China

4 School of Nuclear Science and Technology, University of South China, Hengyang 421001, China

5 University of Chinese Academy of Sciences, Beijing 100049, China

6 School of Physical Science and Technology, ShanghaiTech University, Shanghai 201210, China

At the SLEGS, a large-volume Φ76.2 mm × 101.6 mm $LaBr_3$(Ce) detector, manufactured by Saint-Gobain [10], and a Φ76.2 mm × 200 mm BGO detector were employed to directly monitor the attenuated beam. Indirect methods rely on nuclear reactions induced by γ-rays, such as $d(\gamma, n)p$ in D_2O and deuterated benzene cell (C_6D_6) targets, to monitor the beam flux by counting the neutrons at HIγS. The γ-ray flux calculated at 3 MeV was 1.2×10^7 photons/s with the simulation detector efficiency, and the overall systematic uncertainty could be limited to below 5% [11, 12]. Another indirect method involves Compton scattering by a copper target employed at the ELI-NP to measure the relative beam flux [13]. Additionally, the photon activation method, which involves photon–nuclear reactions such as $^{197}Au(\gamma, n)^{196}Au$, $^{27}Al(\gamma, x;x = 2pn,pd^3He)^{24}Na$ [14–16], $^{93}Nb(\gamma, n)^{92m,g}Nb$, and others, provides another means for determining the beam flux. Specifically, for the LCSS γ-ray beams at the SLEGS, $^{197}Au(\gamma, n)^{196}Au$ and $^{64}Zn(\gamma, n)^{63}Zn$ were selected to measure the γ-ray beam flux. This article is organized as follows. Section 2 introduces the basic principles and methods for Photon Activation Analyses (PAA) [17–19], including the γ-ray beam source and detection system. Section 3 outlines our data analysis procedure. Section 4 discusses the prospects of the PAA, such as the improvement of nuclear reaction data, development of new γ-ray sources, and integration of PAA with other techniques.

2 SLEGS beamline and PAA setup

2.1 γ-ray beam characterization

A laser Compton scatter γ-ray beam was generated in a interaction chamber by employing a CO_2 laser (wavelength: 10.64 μm) operating at a low frequency of 1 kHz, with a pulse width of 50 μm (equivalent to 5 W laser power). This laser beam was collided with a 3.5 GeV electron in the SSRF storage ring, resulting in the production of quasi-monochromatic γ-rays beam with energies varying from 0.66 MeV to 21.7 MeV. The γ-ray beam flux ranged from 4.8×10^5 ph/s to 1.5×10^7 ph/s [1]. The main parameters of the SLEGS are listed in Table 1. The LCSS γ-ray beam was then directed through a vacuum pipeline, passing sequentially through a coarse collimator, fine collimator, and attenuator [20–23] before ultimately reaching the experimental hall. This well-controlled transport setup ensured precise delivery of the γ-ray beam to the experimental hall.

Table 1 (Color online) Parameters for SLEGS operation

parameter	Value	Comments
E-beam bunch interval (ns)	2	
E-beam energy (GeV)	3.5	
E-beam current (mA)	180–210	Top-up mode
γ-ray energy (MeV)	0.66–21.7	CO_2 Laser
Total flux (γ /s)	$4.8 \times 10^5 - 1.5 \times 10^7$	20° − 180°

Figure 1 shows a diagram illustrating the online activation and offline measurements. The activation platform, featuring a multi-slot target holder, was strategically positioned behind the beam pipe exit. A silicon pixel imaging detector (MiniPIX) was used to facilitate beam spot imaging and reaction target localization. Additionally, a Φ76.2 mm × 101.6 mm $LaBr_3$(Ce) detector was placed at the termination point of a LCS γ-ray beamline to measure both the γ-ray beam flux and energy. Figure 2 shows the detector response to γ-ray beam at collision angles of 124° and 132° using a 3 mm coarse collimator under 200 mm copper attenuation. The energy and efficiency calibrations of the $LaBr_3$(Ce) detector were performed using monoenergetic gamma rays from nuclear reactions (6.13 MeV, 9.17 MeV, 10.76 MeV, 17.6 MeV) and the radioactive source ^{60}Co [24–27]. The profile of a quasi-monoenergetic γ-ray beam overlaid on a continuous bremsstrahlung background was clearly visible. Using the unfolding method, the corresponding γ-ray energy spectrum without detector response was successfully solved, as shown in Fig. 2 (pink and blue). The details of the unfolding method for the γ-ray beam are presented in [28].

2.2 Low background HPGe detector systems

The characteristic γ-rays emitted from a nuclide sample were measured using a HPGe detector (ORTEC GEM70200-p). This detector showed a relative efficiency of 55.2% at

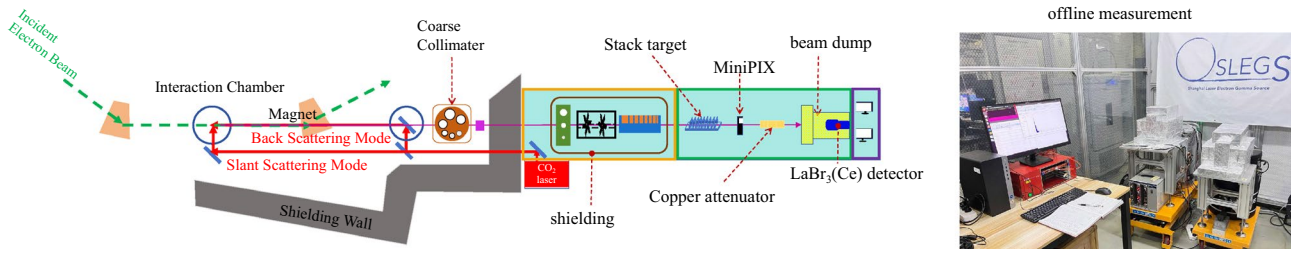

Fig. 1 (Color online) Schematic layout of the SLEGS beamline, online activation, and offline low background HPGe setup

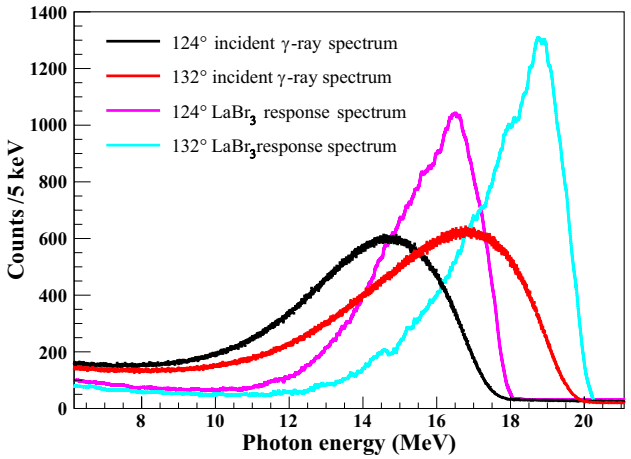

Fig. 2 (Color online) γ-ray energy spectrum measured with a Φ76.2 mm × 101.6 mm $LaBr_3$(Ce) detector. The spectrum was solved by the unfolding method. γ-ray energy spectrum of several laser-electron collision angles measured by a $LaBr_3$(Ce) detector for 124° (black) and 132° (red) (Unfolding γ-ray energy spectrum at the same angles)

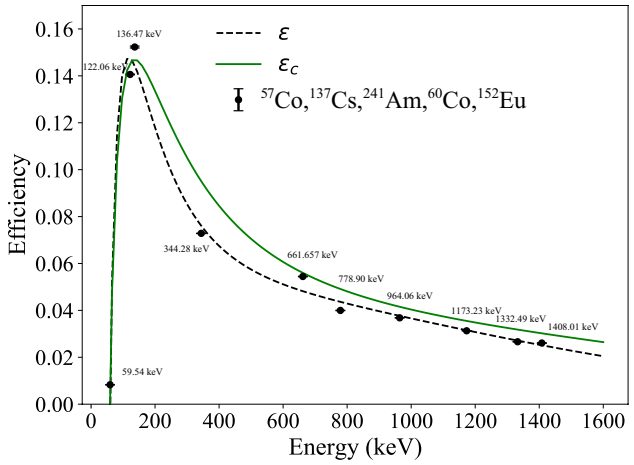

Fig. 3 Fitting curves of the measured and interpolated detector efficiencies

1333 keV and an impressive energy resolution of 5.99 keV at 1333 keV (0.45%). To minimize background interference, 10 cm thick lead shields were employed to ensure low background counts (less than 5 cps) within a range of 60 keV to 3000 keV.

Calibration of the HPGe detector efficiency was meticulously carried out using standard gamma sources, including ^{152}Eu (24.5 kBq), ^{137}Cs (8.177 kBq), ^{57}Co (80.73 kBq), and ^{241}Am (6.516 kBq). The absolute efficiency (η) of the gamma source positioned at an identical distance from the HPGe detector is determined using Eq. (1). This rigorous calibration ensured the accurate and reliable measurement of the activity of the irradiated target.

$$\eta = \frac{NF_{\text{tsc}}}{A_0 e^{-\lambda T} I_0 T_{\text{c}}} \tag{1}$$

Here, N represents the photon peak counts obtained from the standard calibration gamma source, F_{tsc} denotes the correction factor for the coincidence summing effect, A_0 denotes the source activity at the factory, T is the time elapsed from the factory to the present, I_0 denotes the characteristic γ-ray transition relative intensity , and T_{c} is the counting time. To estimate the efficiencies corresponding to the γ-rays emitted from the decay of ^{57}Co, ^{137}Cs, ^{241}Am, ^{60}Co, and ^{152}Eu, a linear parametric model represented by Eq. (2) is employed.

The fitted curves of the interpolated and measured detector efficiencies are shown in Fig. 3. ϵ is the efficiency curve obtained from the experimental data, and ϵ_c is the correction efficiency for summing the coincidence effects. Furthermore, the correction for the summing coincidence effects was accomplished through a Geant4 simulation [29], to ensure accurate corrections and enhance the reliability of the calibration process.

$$\epsilon = e^{a+b(\ln E)+c(\ln E)^2+d(\ln E)^3+e(\ln E)^4+f(\ln E)^5} \tag{2}$$

3 Activation data analysis

Gold, a commonly utilized activated material, was selected for comparison with zinc, a short-lived activated material. In this study, the γ-ray beam flux extracted from the ^{197}Au(γ, n)^{196}Au and ^{64}Zn(γ, n)^{63}Zn reactions was meticulously measured. The measurements spanned from 102° (13.16 MeV) to 139° (19.08 MeV), providing valuable insights into the beam flux characteristics.

3.1 Calculation of the γ-ray beam flux

The γ-ray beam flux $\phi(t)$ is determined using Eq. (3).

$$\phi(t) = \frac{N_\gamma}{\sigma N_A A_b I_\gamma \eta f_{\text{t}} f_{\text{s}}} \tag{3}$$

Here, N_γ is the effective count measured using the HPGe detector. N_A is the number of target nuclei per unit surface, and A_b is the natural isotope abundance of the target. I_γ denotes the characteristic γ-ray transition relative to the target intensity. σ is the average cross section, where $\sigma = \int \sigma(E) n_\gamma(E) \mathrm{d}E$. $n_\gamma(E)$ is the incident γ-ray beam distribution, calculated using the direct unfolding method and combined with the response function ($\boldsymbol{R_f}$) of the $LaBr_3$(Ce) beam monitor simulated by the Geant4 code. The γ-ray

Table 2 Isotope and decay data

Product nuclide	Reaction	S_n (MeV)	$T_{1/2}$	E_γ (keV)	I_γ
^{196g}Au	^{197}Au$(\gamma,n)^{196}$Au	8.073	6.1669 day	355.73	0.87
^{63}Zn	^{64}Zn$(\gamma,n)^{63}$Zn	11.86	38.47 min	511.00	1.855

spectrum ($\boldsymbol{n}_{\rm det}$) was measured by a $LaBr_3$(Ce) detector as detailed in [28]

$$\boldsymbol{n}_{\rm det} = \boldsymbol{R}_f \boldsymbol{n}_\gamma \tag{4}$$

The γ-ray beam energy distribution $\boldsymbol{n}_\gamma$ can be deduced from Eq. 4 via iterative least-squares fitting. We selected the total energy response of the $LaBr_3$(Ce) detector as the zeroth trial function obtained from Eq. 4. Then, we iterated this procedure j times, yielding

$$\boldsymbol{n}_{\rm det}{}^{j} = \boldsymbol{R}_f \boldsymbol{n}_\gamma{}^{j}, \tag{5}$$

$$\boldsymbol{n}_\gamma{}^{j+1} = \boldsymbol{n}_\gamma{}^{j} + (\boldsymbol{n}_{\rm det} - \boldsymbol{n}_{\rm det}{}^{j}). \tag{6}$$

Finally, n_γ was obtained by iterating the program until convergence. The uncertainty of the unfolding method was less than 1%. The total efficiency of the $LaBr_3$(Ce) detector was approximately 84.75% to 87.15% at slant-scattering angles from 102 to 139. The time correction factor $f_{\rm t}$ is shown below.

$$f_{\rm t} = \frac{(1-e^{-\lambda T_{\rm i}})e^{-\lambda T_{\rm w}}(1-e^{-\lambda T_{\rm c}})}{\lambda} \tag{7}$$

Here, λ denotes the decay constant, $T_{\rm i}$ is the irradiation time, and $T_{\rm w}$, called the cooling time, is the elapsed waiting time between the end of irradiation and start of the offline HPGe measurement count.

The self-attenuation coefficients ($f_{\rm s}$) owing to the interactions of the γ-rays within the sample thickness are given by Eq. 8. μ is the attenuation coefficient obtained from NIST [30], and t is the mass thickness.

$$f_{\rm s} = \frac{\mu t}{1-e^{-\mu t}} \tag{8}$$

3.2 Target material for activation

The ^{197}Au$(\gamma,n)^{196}$Au and ^{64}Zn$(\gamma,n)^{63}$Zu reactions were specifically chosen to monitor the γ-ray beam flux at the SLEGS. The single-neutron separation energies for ^{197}Au and ^{64}Zn are 8.073 MeV and 11.86 MeV, respectively. Consequently, for these reactions, the γ-ray beam flux can be effectively monitored within the energy ranges of $8.07-21.00$ MeV and $11.96-25.00$ MeV, respectively, ensuring comprehensive coverage across the desired γ-ray beam energies. They exhibited a broader monitoring energy range, and the giant resonance excitation functions for these reactions are shown in Figs. 4(a) and (b). This presentation encompasses previously reported experimental data from the EXFOR experimental database and evaluated cross sectional data from the ENDF/B-VIII.0 and IAEA/PD-2019 libraries. Owing to their substantial cross sections, these reactions facilitated short activation times, making them versatile for a variety of experiments. The half-lives of ^{196g}Au and ^{63}Zn were 6.1669 days and 38.47 min, respectively.

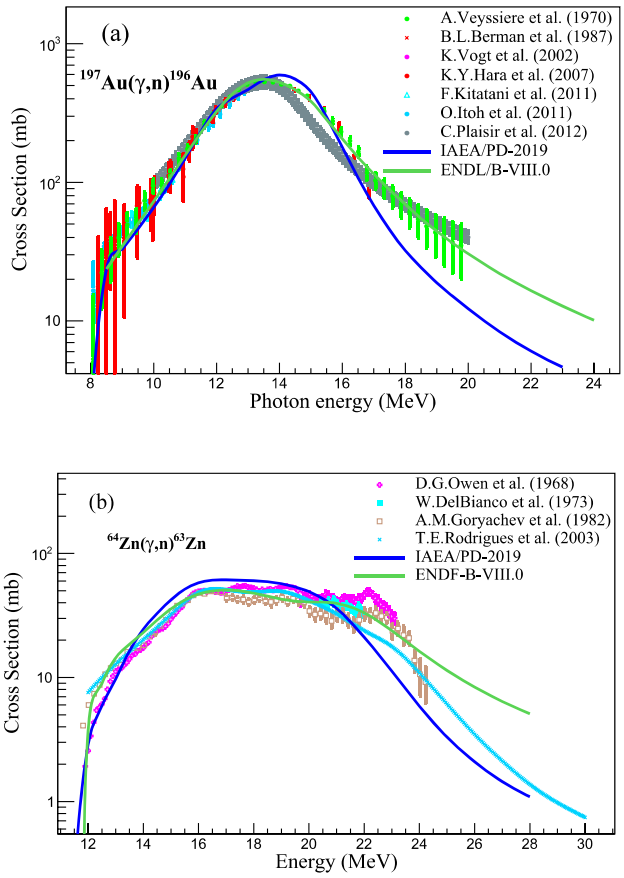

Fig. 4 (Color online) **a** ^{197}Au$(\gamma,n)^{196}$Au cross section as a function of the γ-ray energy from literature [32–40] and evaluated data (ENDF/B-VIII.0 and IAEA/PD-2019). **b** ^{64}Zn$(\gamma,n)^{63}$Zn cross section as a function of the γ-ray energy from literature [41–47] and evaluated data (ENDF/B-VIII.0 and IAEA/PD-2019) [48]

Figure 5 shows the level scheme of ^{196g}Au and ^{63}Zn decays, along with the characteristic γ-ray energies and intensities associated with each. The relative nuclear spectroscopic data were sourced from the NuDat 3.0 database [31].

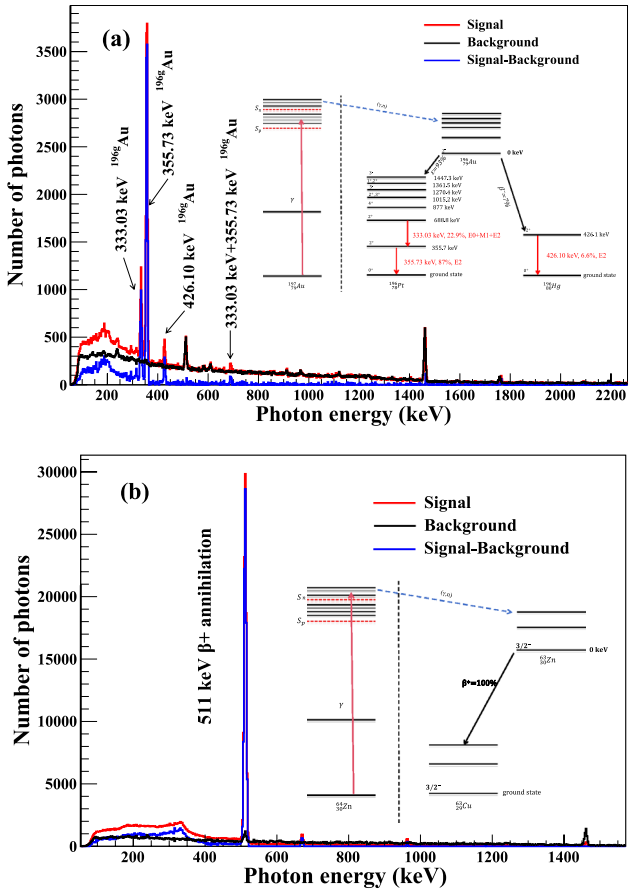

Fig. 5 **a** Typical energy spectra of an Au target irradiated by LCS γ-ray beams ($E_\gamma = 19.08$ MeV). **b** Typical energy spectra of a Zn target irradiated by LCS γ-ray beams ($E_\gamma = 19.08$ MeV)

In addition to their utility in experimental settings, both reactions were well suited for offline measurements.

The beam flux activation monitor utilized a natural gold target (^{197}Au 100%) with a purity of 99.99% and thickness of 0.5 mm. In addition, natural Zn targets (^{64}Zn 49.2%, ^{66}Zn 27.7%, ^{67}Zn 4.0%, ^{68}Zn 18.5%, and ^{70}Zn 0.6%) with a purity of 99.99% and thickness of 2 mm were employed. The target had a diameter of 10 mm, which exceeded the diameter of the γ-ray beam restricted by a 3 mm coarse collimator. The target was strategically positioned on a multi-slot target holder along the beam axis and precisely placed in front of the experimental hall. The target underwent meticulous irradiation using a focused γ-ray beam. This deliberate irradiation resulted in well-controlled ^{197}Au$(\gamma, n)^{196}$Au and ^{64}Zn$(\gamma, n)^{63}$Zn reactions, which played a crucial role in the experimental procedure. The accuracy of cross-section data for nuclear reactions is crucial in beam monitoring. Experimental measurements of cross sections for the ^{197}Au$(\gamma, n)^{196g}$Au reaction [32–40] were conducted using γ-rays produced by several sources, including bremsstrahlung γ-rays [32, 40], positron annihilation in flight-generated quasi-monochromatic γ-rays [33, 34, 39], and LCS-generated quasi-monochromatic γ-rays [35–38]. The experimental cross-section data for the ^{64}Zn$(\gamma,n)^{63}$Zn reaction [41–47] were measured using monoenergetic γ-rays produced by nuclear reactions, including the ^{3}H$(p,\gamma)^{4}$He reaction [41, 47], the ^{7}Li$(p,\gamma)^{8}$Be reaction [45], and bremsstrahlung γ-rays [42–44, 46]. The IAEA provides the evaluated data for photonuclear reactions [48].

The ^{197}Au$(\gamma, n)^{196}$Au reaction produces unstable nuclei, such as ^{196m}Au and ^{196g}Au. Subsequently, ^{196m}Au is de-excited by emitting γ-rays, leading to the formation of ^{196g}Au. The decay of ^{196g}Au proceeds through either electron capture (93%), yielding ^{196}Pt, or through β^- decay (7%), resulting in ^{196}Hg. The decay profiles are shown in Fig. 5(a). Additional reaction details are summarized in Table 2.

3.3 Characteristic γ-ray de-excitation spectrum

The γ-ray beam flux was quantified by identifying the characteristic transition peaks associated with the ground state of ^{196g}Au, following the photon–neutron reaction with ^{197}Au. This ground state of ^{196g}Au has a half-life of 6.1669 days, making it a reliable marker for assessing the strength of the γ-ray beams. The irradiation, cooling, and counting times were carefully selected as $t_i = 0.5637$ days, $T_w = 2.24$, and $T_c = 224,309$ s, respectively. Notably, the cooling time exceeded two days, ensuring 99% decay of the excited state of ^{196m}Au ($E_{level} = 0.5957$ MeV, $T_{1/2} = 9.6$ hours) to reach the ground state. This meticulous time allocation enhanced the reliability and precision of the experimental measurements. Figure 5(a) shows the distinct characteristic the γ-ray transitions resulting from the irradiation of the ^{197}Au target using a 19.08 MeV γ-ray beam. Notably, the characteristic γ-rays of ^{196g}Au include peaks at 355.73 keV and 333.03 keV, originating from the β^- decay of ^{196g}Au, along with the peak at 426.10 keV, corresponding to the inner transition (IT) decay of ^{196g}Au. These features contribute to a comprehensive understanding of the experimental spectra.

^{63}Zn undergoes β^+ decay, resulting in the emission of a characteristic peak at 511 keV because of the annihilation of positrons with electrons. The *gamma*-ray energy spectra recorded for zinc samples irradiated with 19.08 MeV photons are illustrated in Fig. 5(b). The experimental conditions included an irradiation time of $t_i = 2$ h, cooling period of $T_w = 3.1$ min, and counting time of $T_c = 2$ h. Notably, the statistical errors associated with these measurements were all below 1%, highlighting the precision of the experimental data.

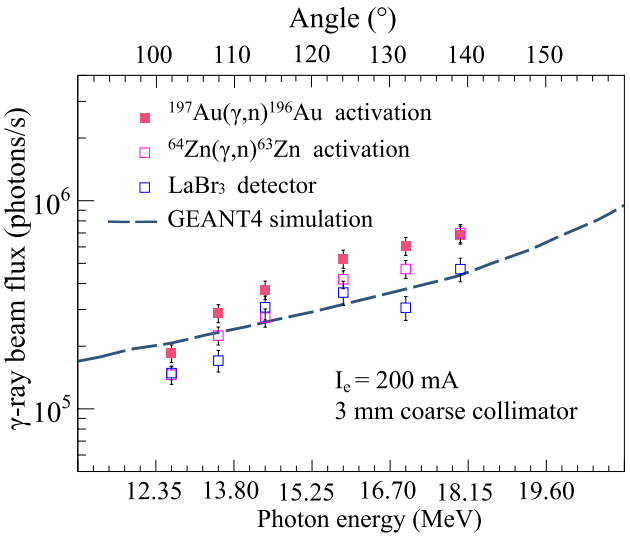

Fig. 6 Comparison of the γ-ray beam flux results from ^{197}Au$(\gamma, n)^{196g+m}$Au and ^{64}Zn$(\gamma, n)^{63}$Zu reactions with the results from direct measurement via the LaBr$_3$(Ce) detector and the Geant4 simulation

4 Results and discussion

The γ-ray beam flux was determined through the activation reactions ^{197}Au$(\gamma, n)^{196g+m}$Au and ^{64}Zn$(\gamma, n)^{63}$Zu, as well as by direct measurements using a LaBr$_3$(Ce) detector. The results presented in Fig. 6, obtained from the activation reactions, exhibit excellent agreement with the LaBr$_3$(Ce) detector and Geant4 simulation outcomes.

Under the conditions of a 3 mm coarse collimator aperture, the γ-ray beam flux ranged from 1.8×10^5 photons/s to 7×10^5 photons/s, depending on the collision angle between the laser and electron beam (ranging from 102° to 139°, corresponding to the γ-ray beam energies of 13.16 – 19.08 MeV). This substantiates the reliability and convenience of the PAA method, proving that it is as effective as classical beam-monitoring methods. When suitable short-lived target materials are utilized, this approach allows for sensitive and rapid online monitoring across different energy regions.

Direct monitoring is challenging at high γ-ray beam flux levels. In such cases, photon activation monitoring is an excellent method for flux indexing. Our group also developed a rapid monitoring method for short-lived target materials, as detailed in subsequent studies. The total uncertainties in the measured γ-ray beam flux for the ^{197}Au$(\gamma, n)^{196g+m}$Au and ^{64}Zn$(\gamma, n)^{63}$Zu reactions and LaBr$_3$(Ce) detectors are listed in Table 3.

The error analysis of the γ-ray beam flux measurements included several factors, including the statistical error of the characteristic γ-ray counts (ϵ_{N_γ}); relative errors of the decay constants (ϵ_λ) taken from literature (0.01%) [49]; the uncertainty of $u(E)$ from the unfolding method, which is less than 1%; and the uncertainty in the ^{197}Au$(\gamma, n)^{196g+m}$Au and ^{64}Zn$(\gamma, n)^{63}$Zn cross sections, which are negligible, as indicated in Fig. 4. However, there is a significant error in the experimentally measured cross sections for the two reaction channels, with some exceeding 10%. To mitigate this, we adopted the IAEA/PD-2019 data from the evaluation database as the standard cross sectional values for the data analysis.

Table 3 Uncertainty errors in the PAA method used

Reaction	ϵ_{N_γ} (%)	ϵ_λ (%)	ϵ_{N_A} [%]	ϵ_{I_γ} (%)	ϵ_η (%)
^{197}Au$(\gamma, n)^{196g+m}$Au	0.69	0.01	0.71	0.028	3.71
^{64}Zn$(\gamma, n)^{63}$Zn	0.72	0.13	0.05	0.09	3.71

The efficiency calibration relative errors of the HPGe detector are denoted by ϵ_η, and the relative errors of the number of targets per unit area (ϵ_{N_A}) are associated with the thickness of the targets. Given that the timing of the experiment has a confidence in the picosecond range, along with irradiation time intervals of at least hours, ϵ_T can be considered negligible. The results are listed in Table 3.

5 Conclusion

A flux monitoring system utilizing PAA was developed for the SLEGS. This system served as a supplementary crosschecking tool for direct measurements. The monitoring system comprised both online activation and offline low background HPGe detector components. In this setup, natural materials such as gold and zinc were selected as the preferred target materials. This choice was based on the relatively short half-lives of ^{196g}Au and ^{63}Zn, which rendered them stable for use at γ-ray flux levels exceeding 10^5 photons/s. The chosen materials were effective within the energy range of 13.16 – 19.08 MeV. This system is particularly beneficial for high-flux γ-ray beam experiments.

Through this newly established flux monitoring system, the SLEGS activity platform enhances its experimental capabilities. This enhancement makes it well-suited for conducting photoneutron cross sectional measurements using quasi-monochromatic energy γ-ray beams.

Acknowledgements The authors thank the SSRF colleagues in the accelerator and beamline engineering departments for their technical support and assistance.

Author contributions All authors contributed to the study conception and design. Material preparation, data collection and analysis were performed by Yu-Xuan Yang, Hong-Wei Wang and Yue Zhang. The first draft of the manuscript was written by Yu-Xuan Yang and all authors

commented on previous versions of the manuscript. All authors read and approved the final manuscript.

Data availability The data that support the findings of this study are openly available in Science Data Bank at https://cstr.cn/31253.11.sciencedb.j00186.00503 and https://www.doi.org/10.57760/sciencedb.j00186.00503.

Declarations

Conflict of interest Hong-Wei Wang is an editorial board member for Nuclear Science and Techniques and was not involved in the editorial review, or the decision to publish this article. All authors declare that there are no Conflict of interest.

References

1. H.W. Wang, G.T. Fan, L.X. Liu et al., Commissioning of laser electron gamma beamline SLEGS at SSRF. Nucl. Sci. Tech. **33**, 87 (2022). https://doi.org/10.1007/s41365-022-01076-0
2. K.J. Chen, L.X. Liu, Z.R. Hao et al., Simulation and test of the SLEGS TOF spectrometer at SSRF. Nucl. Sci. Tech. **34**, 47 (2023). https://doi.org/10.1007/s41365-023-01194-3
3. J.G. Chen, W. Xu, W. Guo et al., An X-ray source based on Compton backscattering of laser and 100 MeV electrons. Nucl. Instrum. Methods A **580**, 1184–1190 (2007). https://doi.org/10.1016/j.nima.2007.07.007
4. J.G. Chen, W. Xu, H.W. Wang et al., A potential photo-transmutation of fission products triggered by Compton backscattering photons. Nucl. Instrum. Methods A **599**, 118–123 (2009). https://doi.org/10.1016/j.nima.2008.10.031
5. W. Guo, W. Xu, J. Chen et al., A high intensity beam line of gamma-rays up to 22 MeV energy based on Compton backscattering. Nucl. Instrum. Methods A **578**, 457–462 (2007). https://doi.org/10.1016/j.nima.2007.05.322
6. Y.X. Yang, W.J. Zhao, X.G. Cao et al., Simulation study on the production of medical radioisotopes ^{186g}Re by photonuclear reaction. Radiat. Phys. Chem. **218**, 111599 (2024). https://doi.org/10.1016/j.radphyschem.2024.111599
7. C.X. Tan, X.X. Li, D.Y. Pang et al., ^{233}Pa(n, γ) cross section extraction using the surrogate reaction ^{232}Th(^{3}He, p) ^{234}Pa involving spin-parity distribution. Phys. Rev. C **109**, 044615 (2024). https://doi.org/10.1103/PhysRevC.109.044615
8. Z.C. Zhu, W. Luo, Z.C. Li et al., Photo-transmutation of long-lived nuclear waste ^{135}Cs by intense compton γ-ray source. Ann. Nucl. Energy **89**, 109–114 (2016). https://doi.org/10.1016/j.anucene.2015.11.017
9. R. Pywell, O. Mavrichi, W. Wurtz et al., Photon flux monitor for a mono-energetic gamma ray source. Nucl. Instrum. Methods A **606**, 517–522 (2009). https://doi.org/10.1016/j.nima.2009.04.014
10. Luxium solutions, formerly Saint-Gobain crystal., https://www.luxiumsolutions.com/news/saint-gobain-crystals-now-luxium-solutions
11. C. Matei, J. Mueller, M. Sikora et al., Investigation of the d(γ, n)p reaction for gamma beam monitoring at ELI-NP. J. Instrum. **11**, P05025–P05025 (2016). https://doi.org/10.1088/1748-0221/11/05/P05025
12. A. Banu, E.G. Meekins, J.A. Silano et al., Photoneutron reaction cross section measurements on ^{94}Mo and ^{90}Zr relevant to the p-Process nucleosynthesis. Phys. Rev. C **99**, 025802 (2019). https://doi.org/10.1103/PhysRevC.99.025802
13. G. Turturica, C. Matei, A. Pappalardo et al., Investigation of compton scattering for gamma beam intensity measurements and perspectives at ELI-NP. Nucl. Instrum. Methods A **921**, 27–32 (2019)
14. V. Di Napoli, D. Margadonna, F. Salvetti et al., Monitor reactions for high energy bremsstrahlung beams. Nucl. Instrum. Methods **93**, 77–81 (1971). https://doi.org/10.1016/0029-554X(71)90140-6
15. A.N. Vodin, O.S. Deiev, I.S. Timchenko et al., Cross-sections for the ^{27}Al(γ, x)^{24} Na multiparticle reaction at $e_{\gamma\max}$= 35–95 MeV. Eur. Phys. J. A **57**, 207 (2021). https://doi.org/10.1140/epja/s10050-021-00483-y
16. M. Wang, D. Wu, H. Lan et al., Cross section measurements of ^{27}Al(γ, x)^{24}Na reactions as monitors for laser-driven bremsstrahlung γ-ray. Nucl. Phys. A **1043**, 122834 (2024). https://doi.org/10.1016/j.nuclphysa.2024.122834
17. C. Segebade, A. Berger, Photon activation analysis. Encycl. Anal. Chem. (2008). https://doi.org/10.1002/9780470027318.a6211.pub2
18. C. Segebade, V.N. Starovoitova, T. Borgwardt et al., Principles, methodologies, and applications of photon activation analysis: a review. J. Radioanal. Nucl. Ch. **312**, 443–459 (2017). https://doi.org/10.1007/s10967-017-5238-6
19. Z.C. Li, Y. Yang, Z.W. Cao et al., Effective extraction of photoneutron cross-section distribution using gamma activation and reaction yield ratio method. Nucl. Sci. Tech. **34**, 170 (2023). https://doi.org/10.1007/s41365-023-01330-z
20. Z.R. Hao, G.T. Fan, H.W. Wang et al., Collimator system of SLEGS beamline at Shanghai Light Source. Nucl. Instrum. Methods A **1013**, 165638 (2021). https://doi.org/10.1016/j.nima.2021.165638
21. Z.R. Hao, G.T. Fan, H.W. Wang et al., A new annular collimator system of SLEGS beamline at Shanghai Light Source. Nucl. Instrum. Methods B **519**, 9–14 (2022). https://doi.org/10.1016/j.nimb.2022.02.010
22. H.H. Xu, G.T. Fan, H.W. Wang et al., Interaction chamber for laser compton slant-scattering in SLEGS beamline at Shanghai Light Source. Nucl. Instrum. Methods A **1033**, 166742 (2022)
23. H.H. Xu, G.T. Fan, H.I. Wu, Interaction chamber design for an energy continuously tunable sub-MeV laser-Compton gamma-ray source. IEEE Trans. Nucl. Sci. **63**, 906–912 (2016). https://doi.org/10.1109/TNS.2015.2496256
24. R.E. Azuma, L.E. Carlson, A.M. Charlesworth et al., A Ge(Li) counter investigation of the γ-ray decay of ^{28}Si produced in the reaction ^{27}Al(p,γ)^{28}Si. Can. J. Phys. **44**, 3075–3081 (1966). https://doi.org/10.1139/p66-253
25. F.L. Liu, C.Y. He, H.R. Wang et al., Thick-target yield of 17.6 MeV γ-ray from the resonant reaction ^{7}Li(p,γ)^{8}Be at E_p = 441 keV. Nucl. Instrum. Methods B **529**, 56–60 (2022). https://doi.org/10.1016/j.nimb.2022.08.005
26. F.L. Liu, W.S. Yang, J.H. Wei et al., Study on γ-ray source from the resonant reaction ^{19}F(p, $\alpha\gamma$)^{16}O at E_p = 340 keV. Chin. Phys. B **29**, 070202 (2020). https://doi.org/10.1088/1674-1056/ab96a0
27. Y.L. Dang, F.L. Liu, G.Y. Fu et al., New measurement of thick target yield for narrow resonance at E_x = 9.17 MeV in the $^{13C(p,\gamma)^{14}}$N reaction*. Chinese Phys. B **28**, 060706 (2019). https://doi.org/10.1088/1674-1056/28/6/060706
28. L.X. Liu, H. Utsunomiya, G.T. Fan et al., Energy profile of laser Compton slant-scattering gamma-ray beams determined by direct unfolding of total-energy responses of a BGO detector. Nucl. Instrum. Methods A **1063**, 169314 (2024). https://doi.org/10.1016/j.nima.2024.169314
29. L.C. He, L.J. Diao, B.H. Sun et al., Summing coincidence correction for γ-ray measurements using the hpge detector with a low background shielding system. Nucl. Instrum. Methods A **880**, 22–27 (2018). https://doi.org/10.1016/j.nima.2017.09.043
30. J.H. Hubbell, S.M. Seltzer, X-ray mass attenuation coefficients: Tables of X-ray mass attenuation coefficients and mass

energy-absorption coefficients from 1 keV to 20 MeV for elements Z = 1 to 92 and 48 additional substances of dosimetric interest. NIST Standard Reference Database 126 . https://doi.org/10.18434/T4D01F
31. National nuclear data center NuDat 3.0., https://www.nndc.bnl.gov/nudat3/
32. C. Plaisir, F. Hannachi, F. Gobet et al., Measurement of the ^{85}Rb(γ, n)^{84m}Rb cross-section in the energy range 10–19 MeV with bremsstrahlung photons. Eur. Phys. J. A **48**, 68 (2012). https://doi.org/10.1140/epja/i2012-12068-7
33. B.L. Berman, R.E. Pywell, S.S. Dietrich et al., Absolute photoneutron cross sections for Zr, I, Pr, Au, and Pb. Phys. Rev. C **36**, 1286–1292 (1987). https://doi.org/10.1103/PhysRevC.36.1286
34. S.C. Fultz, R.L. Bramblett, J.T. Caldwell et al., Photoneutron cross-section measurements on gold using nearly monochromatic photons. Phys. Rev. **127**, 1273–1279 (1962). https://doi.org/10.1103/PhysRev.127.1273
35. K.Y. Hara, H. Harada, F. Kitatani et al., Measurements of the ^{152}Sm(γ, n) cross section with laser-compton scattering γ rays and the photon difference method. J. Nucl. Sci. Technol. **44**, 938–945 (2007). https://doi.org/10.1080/18811248.2007.9711333
36. O. Itoh, H. Utsunomiya, H. Akimune et al., Photoneutron cross sections for au revisited: Measurements with laser compton scattering γ-rays and data reduction by a least-squares method. J. Nucl. Sci. Technol. **48**, 834–840 (2011). https://doi.org/10.1080/18811248.2011.9711766
37. F. Kitatani, H. Harada, S. Goko et al., Measurement of ^{76}Se and ^{78}Se (γ, n) cross sections. J. Nucl. Sci. Technol. **48**, 1017–1024 (2011). https://doi.org/10.1080/18811248.2011.9711787
38. F. Kitatani, H. Harada, S. Goko et al., Measurement of the ^{80} Se(γ, n) cross section using laser-compton scattering γ-rays. J. Nucl. Sci. Technol. **47**, 367–375 (2010). https://doi.org/10.1080/18811248.2010.9711967
39. A. Veyssiere, H. Beil, R. Bergere et al., Photoneutron cross sections of ^{208}Pb and ^{197}Au. Nucl. Phys. A **159**, 561–576 (1970). https://doi.org/10.1016/0375-9474(70)90727-X
40. K. Vogt, P. Mohr, M. Babilon et al., Measurement of the (γ, n) cross section of the nucleus ^{197}Au close above the reaction threshold. Nucl. Phys. A **707**, 241–252 (2002). https://doi.org/10.1016/S0375-9474(02)00922-3
41. W.D. Bianco, S. Kundu, P. Boucher, ^{64}Zn(γ, n)^{63}Zn cross section from 20.4 to 21.9 MeV. Can. J. Phys. **51**, 1302–1303 (1973). https://doi.org/10.1139/p73-173
42. T.E. Rodrigues, J.D.T. Arruda-Neto, Z. Carvalheiro et al., Statistical and direct aspects of decay channels in the giant dipole resonance and quasideuteron energy regions. Phys. Rev. C **68**, 014618 (2003). https://doi.org/10.1103/PhysRevC.68.014618
43. G. Hovhannisyan, T. Bakhshiyan, R. Dallakyan, Photonuclear production of the medical isotope ^{67}Cu. Nucl. Instrum. Methods B **498**, 48–51 (2021). https://doi.org/10.1016/j.nimb.2021.04.016
44. A.M.Goryachev, G.N.Zalesnyy, The studying of the photoneutron reactions cross sections in the region of the giant dipole resonance in zinc, germanium, selenium, and strontium isotopes. Voprosy Teoreticheskoy i Yadernoy Fiziki **8**, (1982)
45. T. Nakamura, K. Takamatsu, K. Fukunaga et al., Absolute Cross Sections of the (γ, n) Reaction for ^{63}Cu, ^{64}Zn and ^{109}Ag. J. Phys. Soc. Jpn. **14**, 693–698 (1959). https://doi.org/10.1143/JPSJ.14.693
46. D. Owen, E. Muirhead, B. Spicer, Structure in the giant resonance of ^{64}Zn and ^{63}Cu. Nucl. Phys. A **122**, 177–183 (1968). https://doi.org/10.1016/0375-9474(68)90711-2
47. W.E. Del Bianco, W.E. Stephens, Photonuclear activation by 20.5-MeV gamma rays. Phys. Rev. **126**, 709–717 (1962). https://doi.org/10.1103/PhysRev.126.709
48. T. Kawano, Y.S. Cho, P. Dimitriou et al., IAEA Photonuclear Data Library 2019. Nucl. Data Sheets **163**, 109–162 (2020). https://doi.org/10.1016/j.nds.2019.12.002
49. X.L. Huang, Nuclear Data Sheets for A = 196. Nucl. Data Sheets **108**, 1093–1286 (2007). https://doi.org/10.1016/j.nds.2007.05.001